

# Liquid Methanol from DFT and DFT/MM Molecular Dynamics Simulations

Nicolas Sieffert,<sup>\*,†</sup> Michael Bühl,<sup>‡</sup> Marie-Pierre Gaigeot,<sup>§,||</sup> and Carole A. Morrison<sup>⊥</sup>

<sup>†</sup>Université Joseph Fourier Grenoble I, CNRS UMR-5250 Département de Chimie Moléculaire, 301 rue de la Chimie, 38041 Grenoble Cedex 9, France

<sup>‡</sup>EaStCHEM School of Chemistry, University of St. Andrews, North Haugh, St. Andrews, Fife KY16 9ST, United Kingdom

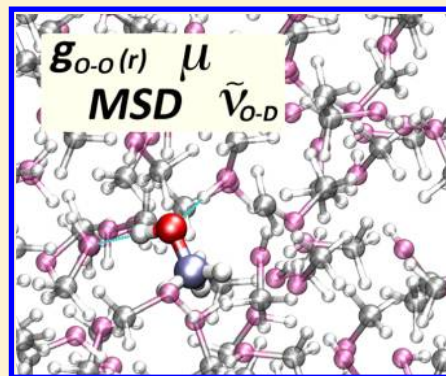
<sup>§</sup>Université d'Evry val d'Essonne, LAMBE UMR8587 Laboratoire Analyse et Modélisation pour la Biologie et l'Environnement, Blvd F. Mitterrand, Bat Maupertuis, 91025 Evry, France

<sup>||</sup>Institut Universitaire de France (IUF), 103 Blvd St Michel, 75005 Paris, France

<sup>⊥</sup>EaStCHEM School of Chemistry, University of Edinburgh, King's Buildings, West Mains Road, Edinburgh, EH9 3JJ, United Kingdom

## S Supporting Information

**ABSTRACT:** We present a comparative study of computational protocols for the description of liquid methanol from *ab initio* molecular dynamics simulations, in view of further applications directed at the modeling of chemical reactivity of organic and organometallic molecules in (explicit) methanol solution. We tested density functional theory molecular dynamics (DFT-MD) in its Car–Parrinello Molecular Dynamics (CPMD) and Quickstep/Born–Oppenheimer MD (CP2K) implementations, employing six popular density functionals with and without corrections for dispersion interactions (namely BLYP, BLYP-D2, BLYP-D3, BP86, BP86-D2, and B97-D2). Selected functionals were also tested within the two QM/MM frameworks implemented in CPMD and CP2K, considering one DFT molecule in a MM environment (described by the OPLS model of methanol). The accuracy of each of these methods at describing the bulk liquid phase under ambient conditions was evaluated by analyzing their ability to reproduce (i) the average structure of the liquid, (ii) the mean squared displacement of methanol molecules, (iii) the average molecular dipole moments, and (iv) the gas-to-liquid red-shift observed in their infrared spectra. We show that it is difficult to find a DFT functional that describes these four properties equally well within full DFT-MD simulations, despite a good overall performance of B97-D2. On the other hand, DFT/MM-MD provides a satisfactory description of the solvent–solute polarization effects with all functionals and thus represents a good alternative for the modeling of methanol solutions in the context of chemical reactivity in an explicit environment.



## INTRODUCTION

Methanol is one of the simplest nonaqueous solvents and is of general interest in chemistry since its polar character and its good hydrogen-bond capabilities make it a versatile medium in which to conduct a broad variety of organic and organometallic reactions. Methanol is also seen as an important reaction substrate in the context of sustainable power management since it can be derived from biomass and used directly in fuel cells.<sup>1</sup> Despite its straightforward molecular structure, complicated arrangements can be afforded in solution due to its “amphiphilic”-like topology, involving a polar O–H group (electrostatic interactions, H-bond donor, and acceptor sites) and an apolar –CH<sub>3</sub> group (van der Waals interactions). In the neat liquid environment, these features give rise to the formation of chains, small cyclic oligomers, or intermediate “lasso”-like structures,<sup>2</sup> whereas in the presence of solutes, complicated solvation patterns can be afforded. As a consequence, the solubility<sup>3</sup> and ion pairing properties<sup>4</sup> of

metal complexes can be strongly affected by the presence of solvating methanol molecules. A proper description of these interactions is mandatory as far as the modeling of the chemical reactivity is concerned, but this question remains a difficult task to address by routine quantum chemical methods, e.g., by performing “static” calculations and using implicit solvation models.<sup>5</sup>

Another approach relies on performing molecular dynamics (MD) simulations in which model solutions (that include explicitly represented solvent molecules) are described in a dynamical ensemble, at a given temperature. This technique allows for a proper description of solvent–solute interactions and avoids any bias being introduced by a polarizable continuum or when minimizing microsolvated clusters in “static” calculations. Pioneering MD studies of Jorgensen<sup>6</sup> and

Received: September 10, 2012

Published: October 30, 2012

Haughney et al.<sup>7</sup> provided the first molecular-level information on the structure and dynamics of neat liquid methanol. A simple model based on an empirical force field was employed, in which molecular interactions were mainly described as a sum of steric and electrostatic interactions over pairs of atoms. This early approach already allowed for a good description of the physicochemical properties of the liquid phase, and recent advances in force field formulations provided interesting improvements, e.g., by including many-body and induced polarization effects.<sup>8</sup> However, the lack of description of bond formation/breaking processes makes classical MD methods unsuited to chemical reactivity studies. This issue is being addressed by the design of the so-called “reactive force fields”<sup>9</sup> or, alternatively, by the use of density functional theory based molecular dynamics (DFT-MD) techniques (sometimes also called *ab initio* MD). The latter has recently emerged as an interesting alternative, since the description of the electronic structure allows for an accurate account of covalent interactions and their related charge transfer and polarization effects. This technique has also been successfully applied to the study of transition-metal catalyzed reactions, where the (explicitly represented) solvent molecules are found to play an active role in the reactivity of the systems.<sup>10</sup>

However, all DFT-MD simulations reported so far on methanol solutions involve the BLYP functional, which is generally not the best choice for the description of solutes, especially as far as transition metal complexes are concerned where both geometries<sup>11</sup> and energies<sup>12</sup> may be associated with notable errors. BLYP is mainly used because it allows for an acceptable description of the structure and dynamics of the solvent under ambient conditions,<sup>13</sup> despite a tendency to yield a somewhat overstructured liquid. A very active research effort still focuses on improving the description of neat liquids by investigating the influence of the density functional and the addition of correction terms to the functional energy to account for long-range dispersion interactions, e.g., following the popular approach developed by Grimme.<sup>14</sup> Such corrections have been already seen as very promising in DFT-MD simulations of liquid water, where properties such as diffusivity<sup>15</sup> and melting point<sup>16</sup> are noticeably improved when going from the pure BLYP functional to its dispersion-corrected “BLYP-D2” or “BLYP-D3” variants.<sup>17</sup> Recently, McGrath et al. evaluated the performance of BLYP-D2 to describe the vapor–liquid phase equilibrium of methanol and also found substantial improvements compared to BLYP results.<sup>18</sup> Their studies also pointed to a significant influence of the choice of the basis set employed in DFT-MD simulations.<sup>18,19</sup> On the other hand, little attention has been paid to density functionals that are traditionally used in inorganic chemistry such as BP86 or the more recently developed B97-D2 functional,<sup>14b</sup> which performs very well in describing geometries and the binding energies of ligands to transition-metal centers.<sup>11,20</sup> Another issue related to full DFT-MD simulations is their substantial computational cost, which limits their applicability to small model systems and thus prevents the study of most of the transition-metal complexes that are actually employed in catalysis. This situation therefore calls for the development of a new computational protocol, in which both the solvent and solute would be properly described, involving a DFT-based method to account for bond breaking/bond formation processes, and a suitable force field for long-range electrostatic and dispersion interactions, resulting in a reasonable computational cost.

Herein, we pursue this goal by two approaches: first, we aim at an accurate description of liquid methanol from full DFT-MD simulations by testing the accuracy of a variety of density functionals at describing the structure and dynamics of the liquid. Special attention is given to the recently developed dispersion-corrected functionals following the DFT-D2<sup>14a,b</sup> and -D3<sup>14c</sup> formalisms from Grimme, and to the BP86, BP86-D2, and B97-D2 functionals, which are generally better suited than BLYP to describe metal complexes. The second approach—which is more computationally efficient—consists of combining these functionals with an empirical force field, within a periodic QM/MM<sup>21</sup> scheme (hereafter denoted DFT/MM-MD). The latter method involves the coupling of multiple partitions of a system, one part being treated at a full DFT(-D) level (i.e., a reactive center), whereas another part (typically the solvent) is described by an empirical force field. This approach gathers the best of both worlds and allows us to choose a DFT functional which properly describes the solute without sacrificing the description of the solvent.

Four protocols are tested herein: two of them rely on a full DFT representation of the systems and are based either on Car–Parrinello Molecular Dynamics (CPMD) or Born–Oppenheimer MD (BOMD) following the Quickstep approach as implemented in the CP2K package. Similar comparative studies between CPMD- and CP2K-based protocols have been reported in the literature in the case of neat water, showing that the results can strongly depend on the choice of e.g. temperature,<sup>22</sup> the MD scheme (CPMD vs BOMD),<sup>23</sup> and the MD parameters (cutoff, basis sets, fictitious electron mass, etc.).<sup>24</sup> In the present study, we thus decided to only vary the nature of the density functional, keeping all the other parameters the same. The two other protocols involve a mixed DFT/MM description of the systems that all consist of a single DFT-represented methanol molecule in an MM methanol environment (1367 molecules in total in a large periodic box). Again, the CPMD and CP2K programs have been compared, and both the CPMD/GROMOS96 interface<sup>25</sup> and the BOMD/MM interface of the CP2K package<sup>26</sup> have been tested.

The accuracy of these computational protocols at reproducing the liquid phase behavior under ambient conditions will be thoroughly validated against the available experimental data, by analyzing their ability to describe (i) the average structure of the liquid, (ii) the mean squared displacement of methanol molecules, (iii) the average molecular dipole moments, and (iv) the gas-to-liquid red-shift observed in their infrared spectra. These data will be compared with the average liquid structure derived from neutron diffraction experiments,<sup>27</sup> the experimental diffusion coefficient,<sup>28</sup> the average dipole moment of liquid methanol,<sup>29</sup> and the experimental infrared (IR) spectra measured in the gas phase<sup>30</sup> and in solution.<sup>31</sup>

## ■ METHODS

**I. Classical “MM” Molecular Dynamics (MD) Simulations.** Classical “MM” molecular dynamics (MD) simulations were performed with the OPLS force field,<sup>32</sup> where the potential energy is described by a sum of bond, angle, and dihedral deformation energies, and pairwise additive 1–6–12 (electrostatic + van der Waals) interactions between non-bonded atoms. Force field parameters stem from the set of Optimized Potentials for Liquid Simulations (OPLS) developed by Jorgensen<sup>6b</sup> (hereafter denoted as the OPLS model), where the methyl group is represented in the united atom

**Table 1. Simulated Systems and Characteristics of the First Peak of the O–O RDF ( $g_{\text{O-O}_{\text{max}}}$  and  $r_{\text{O-O}_{\text{max}}}$  in Å) and Average Temperature  $\langle T \rangle$  (K), As Obtained from DFT-MD Simulations<sup>a</sup>**

entry	functional	method	N	cell length (Å)	$t$ (ps)	$\langle T \rangle$ (K)	$g_{\text{O-O}_{\text{max}}}$	$r_{\text{O-O}_{\text{max}}}(\text{Å})$
	exptl. <sup>b</sup>					298	~3.2	~2.8
1	BLYP	CPMD	32	12.9	32.0	293(17)	4.30	2.74
2	BLYP	CP2K	32	12.9	32.0	293(17)	4.38	2.74
3	BLYP-D2	CPMD	32	12.9	32.0	293(17)	4.10	2.74
4	BLYP-D2	CP2K	32	12.9	32.0	293(17)	4.43	2.70
5	BLYP-D3	CP2K	32	12.9	24.0	292(18)	4.03	2.74
6	BP86	CPMD	32	12.9	32.0	293(17)	4.74	2.66
7	BP86-D2	CPMD	32	12.9	32.0	292(17)	5.26	2.66
8	B97-D2	CP2K	32	12.9	32.0	294(17)	3.79	2.74
9	B97-D2	CP2K	32	12.9	44.0 <sup>c</sup>	291(29)	3.95	2.70
10	B97-D2	CP2K	64	16.3	15.0	291(31)	3.75	2.74

<sup>a</sup>All values are computed over the last 12 ps of MD; standard deviations are given in parentheses. In system 10, averages are taken over the last 6 ps of MD.  $N$  and  $t$  stand for the number of methanol molecules in the system, and the length of the simulation, respectively. <sup>b</sup>From an empirical potential structure refinement (EPSR) computer simulation. Derived from neutron diffraction experiments but based on empirical parameters.<sup>27</sup>

<sup>c</sup>Simulation of system 8 pursued for an additional 12 ps.

approximation (with a mass of 15.030 g·mol<sup>-1</sup>). Cross-terms in van der Waals interactions were constructed using Lorentz–Berthelot mixing rules. The MD simulations were performed using 3D periodic boundary conditions. Nonbonded interactions were calculated using a 10 Å atom-based cutoff, correcting for the long-range electrostatics using the Ewald summation method.<sup>33</sup> For small systems, consisting of 32 methanol molecules, a box size of 12.9 Å has been employed to be consistent with ref 13a. An intermediate system has also been prepared and is composed of 64 methanol molecules in a box of cell length 16.3 Å, as in ref 13b. In the case of the larger system (1367 molecules), the latter was pre-equilibrated in the NPT ensemble for 200 ps ( $T = 293$  K,  $P = 1$  atm) to ensure that a near experimental liquid density was afforded.<sup>34</sup> The MD was then continued for 100 ps in the NVT ensemble. The temperature (293 K) was controlled by coupling to a thermal bath with a relaxation time of 0.2 ps, using the Berendsen algorithm. All hydrogen atoms were substituted by deuterium, all O–D bonds constrained with SHAKE, and the Verlet leapfrog algorithm with a time step of 2 fs was used to integrate the equations of motion. These simulations were performed with the AMBER10 software.<sup>35</sup>

**II. Ab Initio Molecular Dynamics Simulations (DFT-MD).** Full DFT-MD simulations have been performed following both Car–Parrinello and Quickstep/Born–Oppenheimer schemes. In both cases, simulated systems consisted of 32 methanol molecules in a cubic box of cell length 12.9 Å, to which 3D periodic conditions were applied. A larger system, involving 64 methanol molecules in a cubic box of cell length 16.3 Å, has also been simulated in order to make sure that our results are not biased by finite size effects. To maintain the time step and reduce the importance of quantum nuclear effects, hydrogen was substituted with deuterium. For simplicity (and to avoid confusion between the diffusion coefficient  $D$  or the Debye unit) deuterium atoms are referred to as H in the text, although we defer to the labeling D in the discussion of vibrational spectra. All simulations were run in the NVT ensemble, using a single Nosé–Hoover thermostat<sup>36</sup> ( $T = 293$  K, frequency 1800 cm<sup>-1</sup>), and were all started from the same (“classically”) pre-equilibrated box (as described in subsection I above).<sup>37</sup> Unless otherwise indicated, all simulations were run for 32 ps. Due to the great computational cost associated with the calculation of the three-body terms, the system involving

BLYP-D3 has been run for 24 ps, whereas the system involving B97-D2 has been extended up to 44 ps to check for convergence of the simulations. The intermediate system, involving 64 molecules, has been simulated for 15 ps (see Table 1). The following computational details are specific to each program:

**Car–Parrinello Molecular Dynamics (CPMD).** CPMD<sup>38</sup> simulations were performed using the BLYP,<sup>39</sup> BLYP-D2,<sup>14a,b</sup> BP86,<sup>39a,40</sup> and BP86-D2<sup>14a,b</sup> functionals alongside norm-conserving pseudopotentials that had been generated according to the Troullier and Martins procedure<sup>41</sup> and transformed into the Kleinman–Bylander form.<sup>42</sup> Kohn–Sham orbitals were expanded in plane waves at the  $\Gamma$ -point up to a kinetic energy cutoff of 80 Ry. A fictitious electronic mass of 600 au and a time step of 0.121 fs have been employed.

**Born–Oppenheimer/Quickstep Molecular Dynamics (CP2K).** BOMD simulations were performed using the QuickStep module<sup>43</sup> of CP2K,<sup>44</sup> which performs DFT-MD using a dual basis set method. Here, the wave functions are described by a Gaussian basis set while the electron density is described by an auxiliary plane wave basis set. A quadruple- $\zeta$  Gaussian basis set augmented with three sets of d-type and p-type polarization functions (QZV3P) was used.<sup>45</sup> Plane waves were expanded up to a density cutoff of 600 Ry and used in conjunction with the GTH pseudopotentials<sup>46</sup> to describe the core electrons.<sup>47</sup> These calculations were performed using the functionals BLYP, BLYP-D2, and BLYP-D3 (i.e., the original BLYP<sup>39</sup> functional with the “-D2”<sup>14b</sup> and “-D3”<sup>14c</sup> correction of Grimme). Note the so-called “three-body terms” which describe the nonadditive dispersion effects are included in the BLYP-D3 calculation. The BP86,<sup>48</sup> BP86-D2, and B97-D<sup>14b</sup> functionals have also been investigated. For every time step of 0.5 fs, the electronic structure was explicitly quenched to a tolerance of 10<sup>-7</sup> Hartree.<sup>49</sup>

**III. Hybrid DFT/MM Molecular Dynamics Simulations.** The topology and coordinates files of the systems pre-equilibrated with the AMBER package<sup>37</sup> were converted into the GROMOS96 format<sup>50</sup> using the script provided with the CPMD/GROMOS96 source code.<sup>25</sup> The resulting GROMOS96 files were then used in both the CPMD- and CP2K-DFT/MM simulations, in such a way that identical systems were considered by the two programs. In all DFT/MM simulations, the DFT subsystem consists of a (nonperiodic)



cubic box of cell length 12.9 Å containing a single methanol molecule, surrounded by 1366 MM methanol molecules. The global simulation cell is a periodic box of 45.9 Å side length. The systems were equilibrated by performing 12 ps of DFT/MM MD in the NVT ensemble (Nosé–Hoover thermostats<sup>36</sup> with  $T = 293$  K and frequency of  $1800\text{ cm}^{-1}$ ). Production runs were performed in the NVE ensemble for an additional 12 ps.<sup>51</sup> Hydrogen atoms of all (DFT and MM) methanol molecules were replaced by deuterium. For consistency, the MM part of the systems was described using the same OPLS parameters (as described in subsection I), and the same sets of parameters as in each corresponding full DFT-MD protocols were employed to describe the DFT region.

In the two DFT/MM schemes, the interaction between the DFT and MM subsystem is defined as a sum of an electrostatic and a van der Waals contribution. The electrostatic interaction is described by a Coulomb potential modified at short-range in order to avoid the well-known electron spill-out problem. The latter involves additional empirical parameters, namely “covalent radii” of MM atoms (denoted  $r_c$ ). However, due to different formulations of this modified potential in the two programs, the parameters  $r_c$  have to be different, in such a way that CPMD-optimized covalent radii cannot be used with CP2K and *vice versa*.<sup>52</sup> More precisely, the following details differ from one QM/MM protocol to another.

**DFT/MM Simulations Performed with the CPMD Interface.** CPMD-DFT/MM simulations were performed using the GROMOS96 interface<sup>25</sup> of the CPMD program,<sup>38</sup> where the DFT region consists of an isolated system described by the same combination of simulations parameters as in the CPMD DFT-MD simulations detailed above (80 Ry cutoff, Troullier Martins pseudopotentials, fictitious mass of the electrons of 600 au, and a 0.121 fs time step). The periodic images were decoupled using the Martyna–Tuckerman approach.<sup>53</sup> The so-called “NN” and “ESP” domains were defined by a 25 Å and 45 Å cutoff, respectively. Typically, 200 and 725 methanol molecules were included in the “NN” and “ESP” regions, respectively. Built-in values for the covalent radii ( $r_{c,i}$ ) of MM atoms were used.<sup>25a</sup>

**DFT/MM Simulations Performed with the CP2K Interface.** In CP2K-DFT/MM calculations, the energies of the DFT and MM regions were computed using the QuickStep and FIST modules, respectively. The DFT region is described using the same parameters as in CP2K DFT-MD simulations (QZV3P basis set, 600 Ry cutoff, GTH pseudopotentials, 0.5 fs time step; see above). The interaction between QM and MM regions was calculated using the procedure developed by Laino et al.<sup>26</sup> Ten Gaussian functions were used for the Gaussian Expansion of the Electrostatic Potential (GEEP). The periodicity was only applied to the MM box, and the QM images were decoupled using the multipole scheme implemented in CP2K. Covalent radii  $r_{c,a}$  of H and O are set to 0.44 Å and 1.20 Å, respectively. The latter have been optimized for water<sup>26a</sup> but are expected to be transferable from one liquid to another. The covalent radius of “C” (i.e., the united atom describing the methyl group) is set to 1.48 Å, in such a way that  $r_{c,a}(\text{O})/\sigma_{\text{OO}} = r_{c,a}(\text{C})/\sigma_{\text{CC}}$  (where  $\sigma_{\text{OO}}$  and  $\sigma_{\text{CC}}$  are the Lennard-Jones parameters of O and of the methyl group, respectively, from the OPLS force field).

**IV. Trajectories Analysis.** The trajectories were saved every 0.5 fs (CP2K simulations) or 0.605 fs (CPMD simulations) and were analyzed using our own Perl scripts and with the VMD software.<sup>54</sup>

**Average Liquid Structure.** The average structure of the liquid was characterized by the radial distribution functions (RDFs). O–O, O–H<sub>o</sub>, and H<sub>o</sub>–H<sub>o</sub> RDFs have been computed (where H<sub>o</sub> denotes the alcohol hydrogens only) and are noted as  $g_{\text{O-O}}$ ,  $g_{\text{O-H}_o}$ , and  $g_{\text{H}_o\text{-H}_o}$ , respectively. A bin size of 0.04 Å has been employed, and no smoothing function has been applied. Averages have been computed over the last 12 ps of MD for the full DFT-MD and for the DFT/MM simulations. The C–C RDFs ( $g_{\text{C-C}}$ ) were also computed to evaluate the effect of dispersion interactions on the liquid structure.

**Self-Diffusion Coefficient.** The self-diffusion coefficient  $D$  of liquid methanol has been computed from the mean-square displacement (MSD) of the oxygen atoms *via* the Einstein relation:<sup>55</sup>

$$6D = \lim_{t \rightarrow \infty} \frac{d\langle |r(t_0 + t) - r(t_0)|^2 \rangle}{dt}$$

where  $r(t)$  is the position of the O atom at a time  $t$ . Here, the angle brackets denote the MSD averaged over all methanol molecules and all possible time origins. The MSD, and thus  $D$ , was corrected *a posteriori* for the displacement of the center of mass of the system (by subtracting its MSD from the one of the oxygens atoms).

**Dipole Moments.** Dipole moments were computed assuming the electronic charge is concentrated in points located on the centers of the maximally localized Wannier functions (corresponding to electron pairs of bonds or lone pairs).<sup>56</sup> This procedure affords a very simple point-charge model, where the positive atomic charges (screened by the core if present) are placed at the nuclear positions and negative charges of  $-2$  at the positions of the Wannier-function centers (WFCs). The total dipole moment is then calculated from this distribution of point charges. This approach has been used successfully to evaluate the dipole moments of individual water molecules in bulk water<sup>57</sup> and to compute IR spectra of solutes in solution.<sup>58</sup>

Since WFCs are derived from the electronic density, their positions are not influenced by the empirical dispersion corrections that are applied. For instance, when MD trajectories are computed at the BLYP-D2 level, WFCs (and thus the dipole moment) are computed at the pure BLYP level. We ensured that this feature does not induce any bias by comparing the position of WFCs computed using different functionals (namely BLYP, BP86, and B97-D2), for a methanol monomer in its BLYP-optimized gas phase geometry. Distance matrices between all atoms and WFCs were computed and compared to each other. This analysis revealed that almost identical positions of WFCs are found regardless of the choice of the density functional (the maximum difference in atom–WFCs distances is 0.005 Å when going from one functional to another; see Table S1). Such small differences induce a negligible variation of the dipole moment ( $\pm 0.01$  D). This feature was also observed in liquid systems, where similar average dipole moments are found regardless of the functional used to compute the WFCs (see Table S2).

**Infrared Spectra and Vibrational Densities of States (VDOS).** Vibrational Densities of States (VDOS) were obtained by computing the Fourier transform of the velocity autocorrelation functions of the oxygen, carbon, and deuterium atoms.<sup>55</sup> Fourier transformation of the autocorrelation function of the O–D distance has also been computed to assess the gas-to-liquid red shift.

Infrared spectra were computed from the Fourier transform of the dipole moment correlation function:

$$I(\omega) = \frac{2\pi\beta\omega^2}{3cV} \int_{-\infty}^{+\infty} dt \langle \mathbf{M}(t) \cdot \mathbf{M}(0) \rangle \exp(i\omega t)$$

where  $\beta = 1/kT$ ,  $c$  is the speed of light in a vacuum, and  $V$  is the volume ( $12.9 \text{ \AA}^3$ ). The angular brackets indicate a statistical average of the correlation of the dipole moment  $\mathbf{M}$  of the absorbing molecular system.  $\mathbf{M}$  is obtained from the positions of WFCs, computed “on the fly” during MD simulations (every 0.5 fs in CP2K-MD and every 0.605 fs in CPMD simulations). In this formula, we have taken into account a quantum correction factor (multiplying the classical line shape) of the form  $\beta\hbar\omega/(1 - \exp(-\beta\hbar\omega))$ , which was shown to give the most accurate results for calculated IR amplitudes.<sup>58,59</sup> All IR spectra were obtained from MD trajectories computed in the NVE ensemble, over 12 ps, in the gas phase and DFT/MM simulations.<sup>51</sup>

Within CPMD simulations, the fictitious mass of the electrons (here 600 au) has been recognized to strongly influence vibrational frequencies.<sup>60</sup> As high frequencies are the most affected, we found that the signals of O–D stretching modes on all spectra calculated from CPMD trajectories are somewhat red-shifted compared to the ones computed from Born–Oppenheimer MD (CP2K). In order to balance the effect of the fictitious mass on vibrational frequencies, we therefore applied a correcting scaling factor, noted  $s_\nu$ , and defined as

$$s_\nu = \frac{\tilde{\nu}_{\text{OD}}(\text{BOMD})}{\tilde{\nu}_{\text{OD}}(\text{CPMD})} = \frac{2671}{2571} \simeq 1.0389$$

where  $\tilde{\nu}_{\text{OD}}(\text{BOMD})$  and  $\tilde{\nu}_{\text{OD}}(\text{CPMD})$  stand for the vibrational frequencies of the O–D stretching mode as obtained from (i) Born–Oppenheimer MD as implemented in the CPMD program ( $\mu = 0 \text{ au}$ ;  $2671 \text{ cm}^{-1}$ ) and (ii) pure Car–Parrinello MD simulations ( $\mu = 600 \text{ au}$ ;  $2571 \text{ cm}^{-1}$ ), respectively. These simulations were run by considering a single  $\text{CD}_3\text{OD}$  molecule in the gas phase using the BLYP functional, in the NVE ensemble (after a NVT pre-equilibration at 293 K). The obtained spectra, computed from dipole–dipole autocorrelation functions over a 10 ps trajectory, are given in Figure S2 in the Supporting Information. The  $s_\nu$  scaling factor was then applied to “stretch” all VDOS and IR spectra obtained from CPMD trajectories.<sup>61</sup>

## RESULTS AND DISCUSSION

This section is divided into two subsections. We first present the results of full DFT-MD followed by those of the hybrid DFT/MM-MD simulations. In each part, both CPMD and CP2K results are detailed. Characteristics of the full DFT-MD and DFT/MM simulations are gathered in Tables 1–4. The data presented in Tables 3 and 4 are also presented as histograms in Figure 3, in order to facilitate comparisons between the different models.

**1. Full DFT-MD Simulations.** Characteristics of the simulated systems are gathered in Table 1. The average structure and the diffusion properties of the liquid have been analyzed by means of O–O, O–H<sub>o</sub>, H<sub>o</sub>–H<sub>o</sub>, and C–C RDFs (depicted in Figure 1), and by computing the mean squared displacement of the methanol molecules (Figure 2). Since these properties strongly depend on thermodynamic conditions, we also report the average temperature over the period of the

**Table 2.** Coordination Numbers of H and O Atoms in the Liquid Obtained by Integration of the First Peak of the O–H<sub>o</sub> RDF and of the Second Peak of the O–O RDF (Up to 2.4 Å and 3.4 Å, Respectively)<sup>a</sup>

functional	method	O–H <sub>o</sub> RDF			O–O RDF	
		DFT <sup>b</sup>	DFT/MM <sup>c</sup>	DFT/MM <sup>c</sup>	DFT	DFT/MM
		O <sub>DFT</sub> –H <sub>DFT</sub>	O <sub>DFT</sub> –H <sub>MM</sub>	H <sub>DFT</sub> –O <sub>MM</sub>	O <sub>DFT</sub> –O <sub>DFT</sub>	O <sub>DFT</sub> –O <sub>MM</sub>
BLYP	CPMD	1.98	1.12	1.00	2.01	2.20
BLYP	CP2K	1.99	1.83	1.00	2.01	3.45
BLYP-D2	CPMD	1.98			2.04	
BLYP-D2	CP2K	1.99			2.08	
BLYP-D3	CP2K	1.98			2.06	
BP86	CPMD	1.99	1.28	1.00	2.02	2.35
BP86-D2	CPMD	2.00	1.61	1.00	2.09	2.81
B97-D2	CP2K	1.95	1.91	1.04	2.04	3.83

<sup>a</sup>RDFs are computed over the last 12 ps of MD at the full DFT level (average over 32 molecules, entries 1–8 see Table 1), and on a single molecule, over 12 ps, at the DFT/MM level. <sup>b</sup>These values include the intramolecular O–H<sub>o</sub> contribution. <sup>c</sup>The intramolecular O<sub>DFT</sub>–H<sub>DFT</sub> contribution is not counted.

**Table 3.** Dipole Moment (in D) of  $\text{CD}_3\text{OD}$  Molecules in the Gas Phase and in the Liquid: Average Dipole Moments (in D) and Standard Deviations (in Parentheses)

functional	method	$\mu$ (D)	DFT-MD	DFT-MD	DFT/MM-MD
			gas <sup>a</sup>	liquid <sup>b</sup>	liquid <sup>c</sup>
exptl.			1.69 <sup>d</sup>	2.87 <sup>e</sup>	2.87 <sup>e</sup>
BLYP	CPMD		1.79(10)	2.71(29)	2.41(19)
BLYP	CP2K		1.78(7)	2.71(27)	2.56(25)
BLYP-D2	CPMD		1.74(7)	2.68(36)	
BLYP-D2	CP2K		1.79(7)	2.72(33)	
BLYP-D3	CP2K		1.79(9)	2.69(31)	
BP86	CPMD		1.69(10)	2.80(32)	2.46(20)
BP86-D2	CPMD		1.70(11)	2.84(36)	2.47(22)
B97-D2	CP2K		1.76(11)	2.58(36) <sup>f</sup>	2.67(23)

<sup>a</sup>A single (isolated)  $\text{CD}_3\text{OD}$  molecule described at a DFT level in a ( $12.9 \text{ \AA}$ )<sup>3</sup> cubic box. Dipole moment of methanol is computed on the fly every 0.5 fs (CP2K) or 0.605 fs (CPMD) of MD and averaged over the last 12 ps of MD. <sup>b</sup>On system containing 32 molecules (see entries 1–8 in Table 1). Dipole moments are averaged over all molecules on 240 snapshots (over the last 12 ps of MD) and are all computed from WFCs at the BLYP level. <sup>c</sup>A single  $\text{CD}_3\text{OD}$  molecule described at a DFT level, surrounded by 1366 MM methanol molecules, level in a ( $45.9 \text{ \AA}$ )<sup>3</sup> cubic box. Dipole moment of the DFT-represented methanol molecule is computed on the fly every 0.5 fs (CP2K) or 0.605 fs (CPMD) of MD, and averaged over the last 12 ps of MD. <sup>d</sup>From ref 62. <sup>e</sup>From ref 29. <sup>f</sup>A dipole moment of 2.59(32) D is obtained in the larger system containing 64 molecules (average of 120 snapshots over the last 6 ps of MD, see entry 10 in Table 1).

analysis for every liquid system. As shown in Table 1, the latter ranges from 291 to 294 K with a standard deviation of 17 to 31 K. Comparisons from one system to another are therefore expected to be meaningful since the average temperature is similar.

**1.1. Average Liquid Structure.** The analysis of the height of the first peak of the O–O radial distribution function (noted  $g_{\text{O–O}_{\text{max}}}$ ) reveals a marked overstructuring of the liquid in all the systems ( $g_{\text{O–O}_{\text{max}}}$  is systematically greater than the reference value 3.2,<sup>27</sup> see Table 1).<sup>23</sup> With BLYP, the

**Table 4. Influence of the Environment on the O–D Stretching Mode of CD<sub>3</sub>OD: O–D Stretching Vibrational Frequencies (in cm<sup>−1</sup>), Computed from the Fourier Transform of the Autocorrelation Function of the O–D Distance [And from Dipole Autocorrelation Function; in Square Brackets] over the Last 12 ps of MD**

$\tilde{\nu}_{\text{O-D}}$ (cm <sup>−1</sup> )		DFT-MD	DFT-MD	DFT/MM-MD
functional	method	gas <sup>a</sup>	liquid <sup>b</sup>	liquid <sup>c</sup>
exptl.		2705 <sup>d</sup>	2491 <sup>e</sup>	2491 <sup>e</sup>
BLYP	CPMD <sup>f</sup>	2671 [2671]	2455	2506 [2507]
BLYP	CP2K	2686 [2680]	2419	2564 [2570]
BLYP-D2	CPMD <sup>f</sup>	2671 [2670]	2448 <sup>g</sup>	
BLYP-D2	CP2K	2679 [2676]	2448 <sup>g</sup>	
BLYP-D3	CP2K	2678 [2685]	2444	
BP86	CPMD <sup>f</sup>	2705 [2705]	2401 <sup>g</sup>	2501 [2501]
BP86-D2	CPMD <sup>f</sup>	2705 [2704]	2433 <sup>g</sup>	2503 [2500]
B97-D2	CP2K	2759 [2760]	2500	2653 [2653] <sup>g</sup>

<sup>a</sup>Considering an isolated CD<sub>3</sub>OD molecule described at a DFT level in a (12.9 Å)<sup>3</sup> cubic box in the NVE ensemble. <sup>b</sup>Considering 32 CD<sub>3</sub>OD molecules described at a DFT level in a (12.9 Å)<sup>3</sup> cubic box, in the NVT ensemble (entries 1–8 in Table 1). <sup>c</sup>Considering a single CD<sub>3</sub>OD molecule described at a DFT level, surrounded by 1366 MM methanol molecules in a (45.9 Å)<sup>3</sup> cubic box in the NVE ensemble. <sup>d</sup>From ref 30. <sup>e</sup>From ref 31. <sup>f</sup>The  $s_v$  scaling factor has been applied to all frequencies obtained from CPMD trajectories to correct the bias induced by the fictitious electron mass (see Methods section and Figure S2 for details). <sup>g</sup>The peak is split in two. The reported value is the average between the two peaks (see Figure S3).

CPMD- and CP2K- protocols give large values (4.30 and 4.38, respectively) and the position of the peak (at *ca.* 2.74 Å) is also slightly shifted toward shorter distances compared to the experiment (*ca.* 2.80 Å). Such features have already been obtained in previous DFT-MD simulations involving different simulation protocols (all based on BLYP).<sup>13b–e</sup> The addition of a dispersion correction is found to have little effect on the overstructuring of the liquid as  $g_{\text{O-O}_{\text{max}}}$  ranges from 4.03 to 4.43 when adding either the “-D2” or “-D3” correction and the position of the peak remain virtually unaffected (see Figure 1 and Table 1). This behavior somewhat contrasts with recent results reported by Siepmann et al., in two separate studies, where they found a decrease in  $g_{\text{O-O}_{\text{max}}}$  from 4.0 to 3.5 when going from BLYP (CP2K protocol involving a cutoff of 280 Ry)<sup>13c</sup> to BLYP-D2 (CP2K protocol with a larger cutoff of 600 Ry).<sup>19</sup> An even larger overstructuring of the liquid is obtained with the BP86 and BP86-D2 functionals ( $g_{\text{O-O}_{\text{max}}} = 4.74$  and 5.26, respectively). The  $g_{\text{O-O}}$  peak is shifted to 2.66 Å and thus exhibits a greater deviation from the experiments (2.80 Å). On the other hand, B97-D2 seems to afford a softer structure as  $g_{\text{O-O}_{\text{max}}}$  is 3.79 in this case and is thus the closest to the experiments. The position of the peak is only slightly shifted (at 2.74 Å). An estimate of the fluctuations of  $g_{\text{O-O}_{\text{max}}}$  in systems of 32 molecules has been obtained by repeating the calculation of the O–O RDF after pursuing the MD for an additional 12 ps, and we found a deviation of 0.16 (compare entries 8 and 9 in Table 1). Moreover, the good performance of B97-D2 is also confirmed by considering a larger system of 64 molecules which shows that very similar RDFs are obtained in this case (compare “B97-D2” and “B97-D2 64” in Figure 1). Similar trends and features are observed in  $g_{\text{O-H}_o}$  and  $g_{\text{H}_o-\text{H}_o}$ .

The integration of the first peak of the O–O RDF (up to 3.4 Å, see Table 2) and of the second peak of O–H<sub>o</sub> RDF (up to 2.4 Å) is consistent with two nearest neighbors per methanol

molecule (on average), each forming one hydrogen bond interaction. The analysis of the C–C RDFs provides interesting insight into the effect of the inclusion of dispersion interactions. As shown in Figure 1, BLYP-D2, BLYP-D3, and BP86-D2 tend to afford peaks that are slightly shifted toward shorter distances compared to their noncorrected counterparts. However, this effect is rather small in magnitude.

**1.2. Diffusion of Methanol Molecules.** Insights into the transport properties of methanol can be gained by computing the mean squared displacement of oxygen atoms (see Figure 2a–c). To improve statistics, the latter is averaged over all molecules and all possible time origins.<sup>55</sup> Following this approach, the statistics thus get weaker as the time increases, and more reliable data should be provided at the shortest time. To estimate up to which time the statistics can be considered as reasonable, we recomputed the MSD over a longer trajectory of 44 ps, and we found that the period ranging from  $t = 0$  to 16 ps is equally well described regardless of the length of the trajectory (see Figure 2c, in the case of B97-D2). Graphical comparison of the MSD for the eight combinations of functionals/protocols over this period (Figure 2a and b) shows that BLYP provides the smallest MSD. The addition of a dispersion correction seems to be beneficial as greater MSDs are found with BLYP-D2 and BLYP-D3, which is reminiscent of recent results on liquid water involving BLYP.<sup>15</sup> However, this effect does not appear to be systematic with all functionals as the MSD from BP86 is little affected by the addition of the -D2 correction. We also note that, at short times, BP86, BP86-D2, and B97-D2 provide very similar MSDs (see Figure 2b).

For a tentative comparison with the experiments, the self-diffusion coefficient of methanol can be computed by averaging over the “horizontal” part of  $\text{MSD}(t)/6t$  (see Figure 2d) and applying the Einstein equation. However, the latter is only valid at long times and therefore requires a full convergence of this quantity.<sup>55</sup> As shown in Figure 2d, 44 ps of MD (and *a fortiori* 32 ps) is not sufficient to obtain such convergence, and the comparison with the experiment is thus difficult. Interestingly, Siepmann et al.<sup>23</sup> pointed out that, in the case of water, simulation of more than 500 ps should be required to compute reliable values of the self-diffusion coefficient under ambient conditions, which is beyond the times accessible by present-day DFT-MD simulations. However, Figure 2d clearly suggests that B97-D2 yields a too sluggish liquid, as the computed self-diffusion coefficient is almost half the experimental value. This situation is expected to be worse with BLYP where the slope of the MSD is smaller at short times. On a more positive note, there is no indication from Figure 2a–c that the MSD would reach a plateau (within 32–44 ps), and therefore none of the studied protocols seem to yield a glassy state.

**1.3. Average Dipole Moment and IR Spectrum.** In solution, the dipole moment of methanol is larger than the intrinsic gas-phase value (2.87 D<sup>29</sup> vs 1.69 D;<sup>62</sup> see Table 3 and Figure 3) due to induced polarization stemming from the environment.<sup>8a</sup> In order to assess whether this effect is reproduced in our simulations, we first computed the average molecular dipole of a single methanol molecule in the gas phase, using the same simulation parameters as for the liquid systems. As shown in Table 3, we found that the dipole moment of gas phase molecules is rather well reproduced by all functionals, the deviation with the experiment being only *ca.* 0.1 D (i.e., on the same order of magnitude as the standard deviation). We note that the latter is little affected by the addition of dispersion corrections. As expected, the average dipole moment is



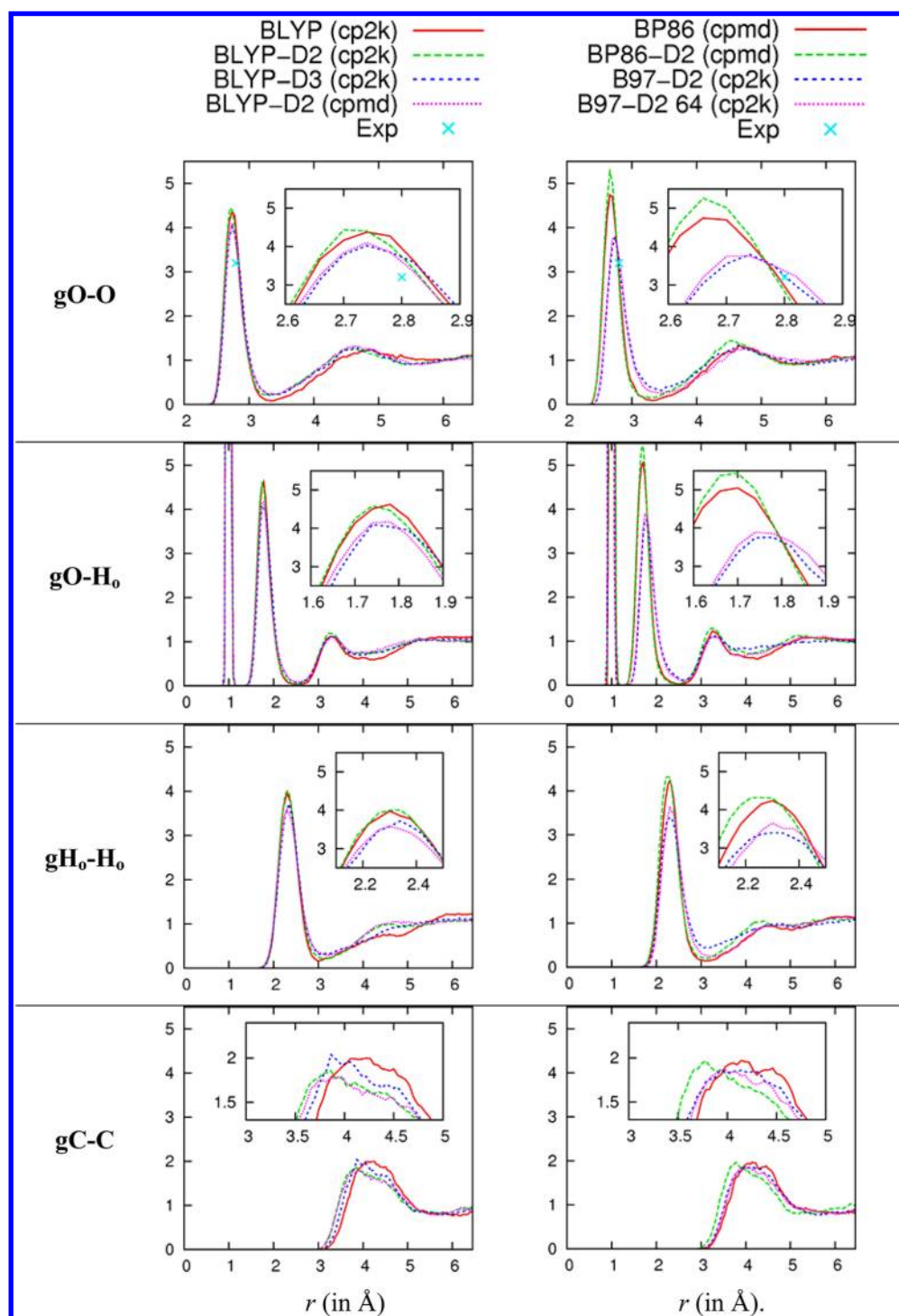


**Figure 1.** Radial distribution functions obtained from DFT-MD simulations using the BLYP, BLYP-D2, and BLYP-D3 functionals (*left column*) and the BP86, BP86-D2, and B97-D2 functionals (*right column*, see entries 1, 3–8, and 10 in Table 1). Taken over the last 12 ps of MD after 20 ps of equilibration.  $r$  (in Å). “Exp” stands for the maximum of the first peak of the O–O RDF from ref 27. “B97-D2 64” denotes the results obtained on the larger system composed of 64 molecules (RDFs are taken over 6 ps in this case; see entry 10 in Table 1).

substantially increased in the case of liquid systems. The experimental dipole moment of liquid methanol (2.87 D) is slightly underestimated, however, in keeping with the results of previous DFT-MD simulations.<sup>13a,b,d</sup> Computed values range from 2.58 to 2.84 D, and the difference observed when going from one functional to another is thus within the typical standard deviation (*ca.* 0.30 D). The choice of protocol and, more importantly, the nature of the density functional therefore

seem to have only a small effect on the description of induced polarization effects, and all protocols tested herein perform rather well.

The environment effects can also be probed by analysis of the vibrational features of the methanol molecules, as it is well-known that a red shift in the stretching O–D vibrational frequency ( $\tilde{\nu}_{\text{O-D}}$ ) is observed when going from the gas phase to the liquid. We therefore computed  $\tilde{\nu}_{\text{O-D}}$  by performing the

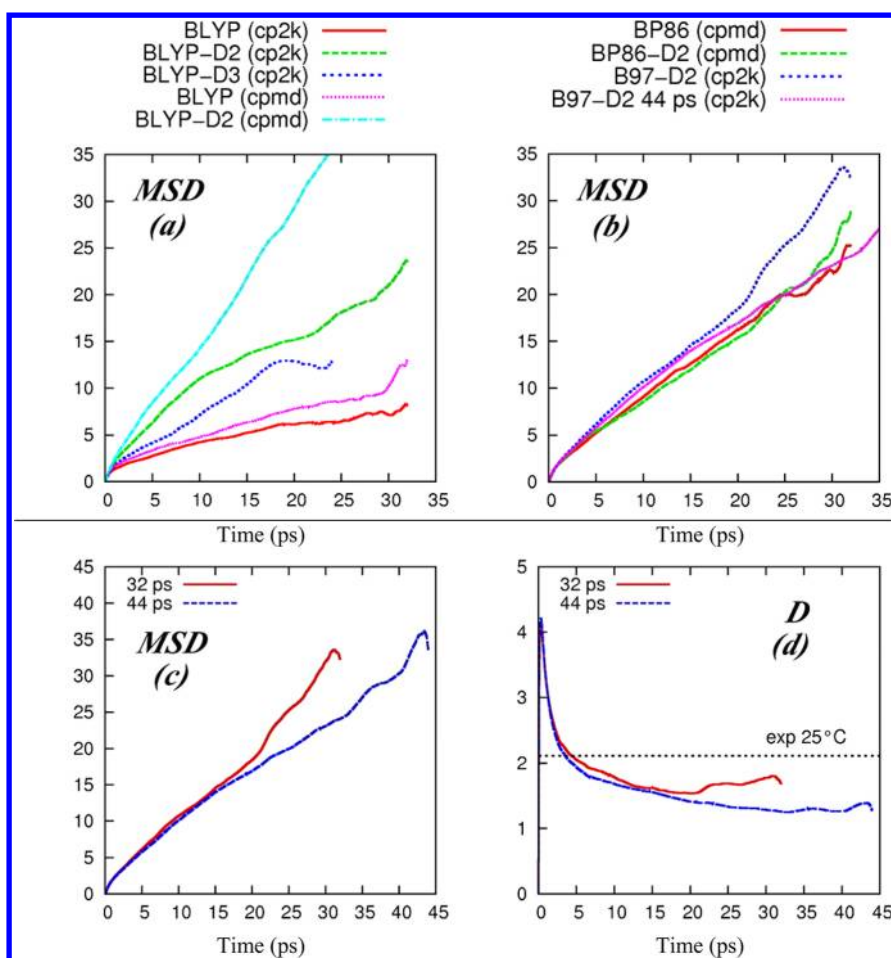


**Figure 2.** Time evolution (ps) of the Mean Squared Displacement (MSD, in  $\text{\AA}^2$ ) and diffusion coefficient ( $D$ , in  $10^{-9} \text{ m}^2/\text{s}$ ) of oxygen atoms in liquid  $\text{CD}_3\text{OD}$ , as obtained from DFT-MD simulations at  $20^\circ\text{C}$ . The MSD of the center of mass has been subtracted. (a and b) A comparison of density functionals (MSD computed over 32 ps, entries 1–8 in Table 1). “B97-D2 44 ps” stands for the MSD obtained on a longer trajectory of 44 ps (entry 9 in Table 1; the full curve is given in c). (c) Comparison between the MSD computed on 32 ps vs 44 ps, at the B97-D2 level (entries 8 and 9 in Table 1). (d) The diffusion coefficient defined as  $D(t) = \text{MSD}(t)/6t$ .

Fourier transformation of the autocorrelation function of O–D distances, both in the gas phase and in the liquid, for each functional/protocol combinations. The vibrational frequencies obtained by this approach have been confirmed by (i) the computation of the full infrared spectra in the case of gas phase molecules (obtained from autocorrelation functions of the dipole moment, see values in square brackets in Table 4 and the Methods section for computational details) or (ii) the computation of vibrational densities of states (VDOS) from velocities’ autocorrelation functions, in the  $1600\text{--}3000 \text{ cm}^{-1}$  domain, in case of liquid systems. Spectra obtained at the B97-D2 level are shown in Figure 4, and all other spectra (obtained in the liquid phase) are provided in Figure S3 in the Supporting Information.

The resulting  $\tilde{\nu}_{\text{O-D}}$  value ranges from  $2671$  to  $2759 \text{ cm}^{-1}$  in the gas phase and therefore exhibits a noticeable sensitivity to the nature of the density functional. BLYP (and its dispersion-corrected versions) tends to underestimate the vibrational frequency slightly, by *ca.*  $30 \text{ cm}^{-1}$ , whereas BP86 (and BP86-D2) reproduces the experimental value very well. On the other hand, B97-D2 provides a slightly worse description of the O–D vibrational frequency since  $\tilde{\nu}_{\text{O-D}}$  is overestimated by  $54 \text{ cm}^{-1}$  in this case (see Figure 4).<sup>63</sup> When going to solution, the red shift is found to be qualitatively well reproduced throughout, despite

a clear tendency to underestimate  $\tilde{\nu}_{\text{O-D}}$  by *ca.*  $50 \text{ cm}^{-1}$ .<sup>64</sup> The value closest to experimental results is obtained with B97-D2 ( $2500 \text{ cm}^{-1}$ ) where the  $\tilde{\nu}_{\text{O-D}}$  band is centered around the experimental value ( $2491 \text{ cm}^{-1}$ ,<sup>31</sup> see Figure 4). On the other hand, BP86 shows the greatest deviation compared to the experimental results and underestimates  $\tilde{\nu}_{\text{O-D}}$  by *ca.*  $90 \text{ cm}^{-1}$ . We note that liquid values may be associated with a rather large uncertainty since broad peaks are obtained and their maximum can be ill defined (averages between maxima have been considered in cases of split peaks; see Figure S3). However, the good description provided by B97-D2 in the liquid is confirmed by considering a larger system (containing 64 molecules), where the  $\tilde{\nu}_{\text{O-D}}$  band is again centered on the experimental value, consistent with the results obtained with the system of 32 molecules (see Figure 4). When comparing this result to those from other functionals, it appears that B97-D2 may benefit from fortuitous error cancellation, as the exaggerated red shift generally found in the liquid (*ca.*  $-50 \text{ cm}^{-1}$ ) is balanced by an intrinsically greater  $\tilde{\nu}_{\text{O-D}}$  vibrational frequency ( $+54 \text{ cm}^{-1}$ ). To summarize, our results converge to the conclusion that the gas-to-liquid red shift is rather well reproduced by DFT-MD simulations, with the B97-D2 functional providing the best description of the vibrational features of liquid methanol (see histogram in Figure 3).



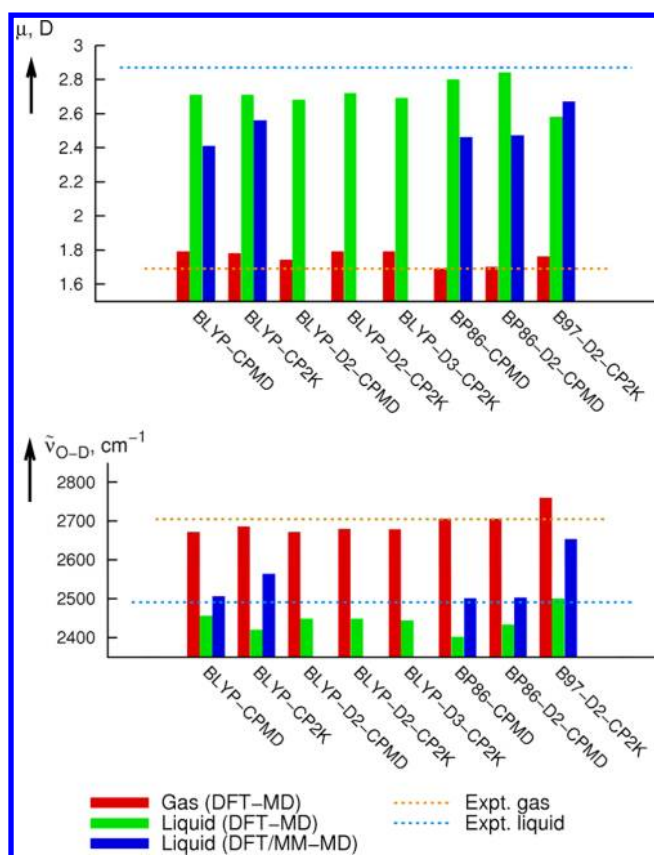


**Figure 3.** Dipole moments (in D; top) and O–D stretching vibrational frequencies (in  $\text{cm}^{-1}$ ; bottom) of gas phase and liquid methanol. Corresponding values are reported in Tables 3 and 4.

**2. Mixed DFT/MM-MD Simulations of Liquid Methanol.** The systems presented in this section are significantly larger and all consist of a single methanol molecule represented on a DFT level, surrounded by 1366 molecules described on a MM level, in a  $(45.9 \text{ \AA})^3$  box. Consistent with the full DFT-MD simulations presented above, analyses were performed over 12 ps. Here, the MSD of the DFT monomer in the MM environment has not been investigated, and we focus on the RDFs, average dipole moments, and  $\tilde{\nu}_{\text{O-D}}$  red shifts as criteria to assess whether the DFT-represented molecule effectively possesses the characteristics of a “liquid molecule” or those of an isolated one (i.e., as found in the gas phase).

**2.1. Average Structure of the Liquid around the DFT Molecule.** The organization of the MM molecules around the DFT monomer strongly relies on empirical parameters, namely, Lennard-Jones parameters and covalent radii ( $r_{\text{c}}$  and  $r_{\text{c,a}}$ ) used in the calculation of the interaction between the two regions. Lennard-Jones parameters are identical in CPMD and CP2K, whereas the sizes of covalent radii depend on the implementation (see the Methods section). Their validity is evaluated herein by comparison between full DFT and mixed DFT/MM simulations at the same level. In the liquid, the CPMD and CP2K protocols exhibit marked differences (compare left and right columns in Figure 5), whereas changing the nature of the functional has virtually no influence (compare e.g. BLYP vs BP86 with CPMD). The addition of the dispersion correction also has a negligible effect (see BP86 vs BP86-D2). We found that the position of the second peak of the O–H<sub>0</sub> RDF is different according to whether the nearest neighbor is the hydrogen bond donor or the acceptor. With CPMD,  $H_{\text{DFT}}\text{--}O_{\text{MM}}$  is shorter than  $O_{\text{DFT}}\text{--}H_{\text{MM}}$  on the average and brackets the  $O_{\text{DFT}}\text{--}H_{\text{DFT}}$  distance (i.e., as obtained from full DFT-MD on the same level). This situation is reminiscent of previous results on liquid water using the same  $r_{\text{c}}$

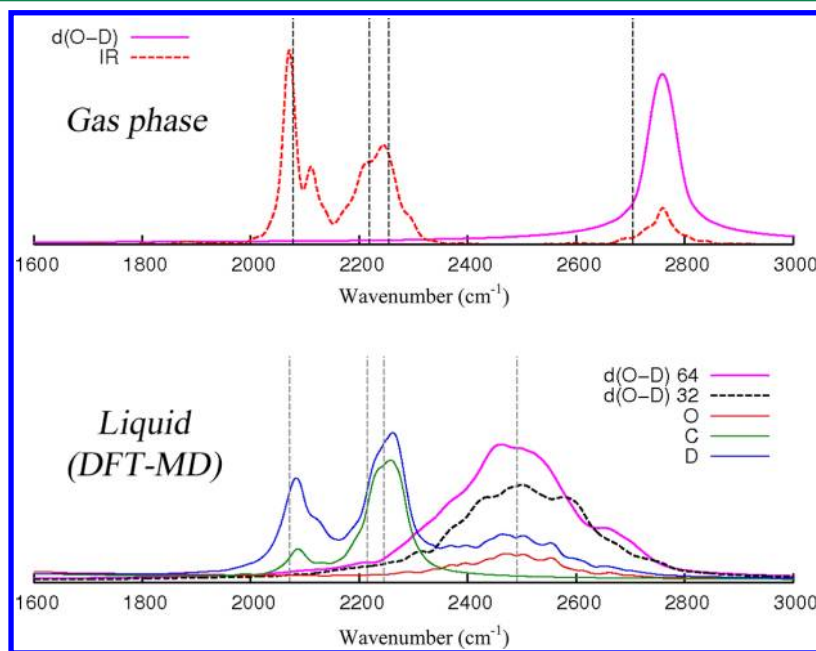


**Figure 4.** Vibrational spectra of gas phase and liquid  $\text{CD}_3\text{OD}$  computed using the B97-D2 functional. “d(O–D)” denotes peaks obtained from the Fourier transformation of the O–D distance autocorrelation functions. “IR” indicates the spectrum computed from dipole autocorrelation functions. For the liquid, d(O–D) spectra of the system containing 64 molecules (labeled “64”, entry 10 in Table 1) and 32 molecules (“32”, entry 8) are reported. “O”, “C”, and “D” denote the VDOS (from the velocities autocorrelation functions) of these atoms in the larger system (entry 10). Vertical dashed lines are the position of the peaks as found from the experiments (see text).

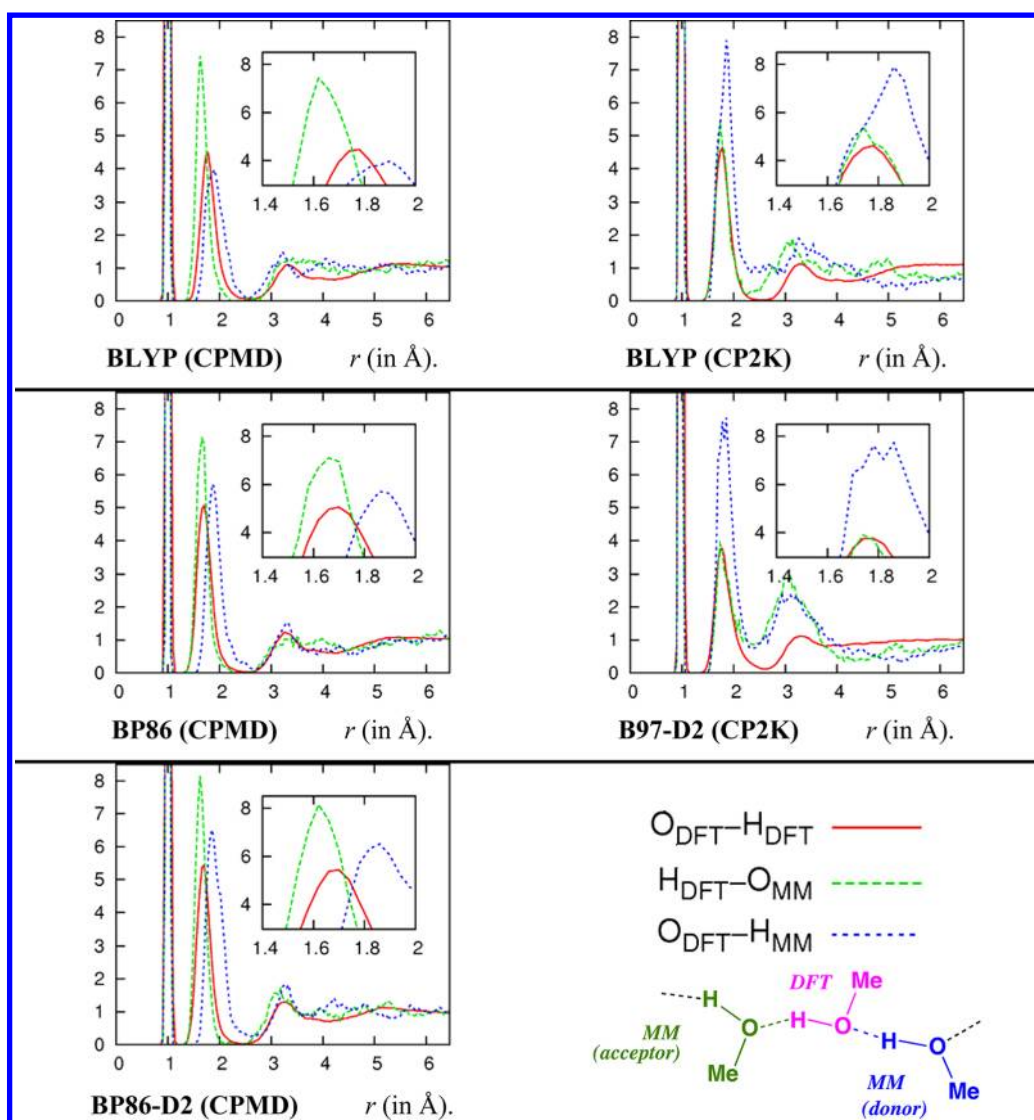


**Figure 5.** Average structure of the MM liquid around a single DFT-represented methanol molecule. O–H<sub>0</sub> radial distribution functions as obtained from full DFT (red; over the last 12 ps of MD) and DFT/MM simulations (green and blue, over the last 12 ps of MD).

parameters.<sup>25a</sup> Integration of the first two peaks also shows marked differences between the two situations, since 1.12 to 1.61 MM molecules on average form hydrogen bonds with O<sub>DFT</sub>, whereas H<sub>DFT</sub> is bonded to a single O<sub>MM</sub> neighbor regardless of the nature of the functional. This result therefore indicates that the DFT molecule is bonded to a single MM acceptor but accepts hydrogen bonds from 1 to 2 MM donors on average.

The same trend is observed with CP2K. The position (and height) of the second peak of the H<sub>DFT</sub>–O<sub>MM</sub> RDF is in good agreement with full DFT-MD, but the O<sub>DFT</sub>–H<sub>MM</sub> RDF still exhibits a broad peak shifted toward longer distances. Again, this feature should mainly stem from the choice of  $r_{c,a}$  parameters and has already been observed in the case of liquid water.<sup>26b</sup> Integration of these peaks also shows that the number of MM hydrogen bond donors is overestimated compared to full DFT-MD, in keeping with the CPMD DFT/MM results. Apparently the directionality of the O<sub>DFT</sub>–H<sub>MM</sub> hydrogen bond interaction is not accurately described, a feature that may be due to the shortcoming of the electrostatic coupling between the electron density of the DFT monomer and the point charges of the MM environment. Such a “simplistic” coupling

also fails to account for the weak covalent contribution existing in hydrogen bonds.<sup>65</sup> This discrepancy could be avoided by using a different QM/MM partitioning of the system, as proposed by Morrone and Tuckerman, where all –OH groups are described at a DFT level whereas the methyl groups are described classically.<sup>66</sup> However, this approach involves cutting the rather polar C–O bonds and introducing link atoms and would remain quite expensive in cases where large simulation boxes are needed.

**2.2. Average Dipole Moment and IR Spectrum of the DFT Molecule.** In order to further evaluate the quality of the QM/MM coupling, we repeated our analysis of the induced polarization effects in solution, by computing the average dipole moment of the DFT-represented monomer in the field of the MM molecules. As shown in Table 3 and Figure 3, the latter ranges from 2.41 to 2.67 D and is therefore underestimated compared to the experimental value (2.87 D)<sup>29</sup> but is still comparable to the full DFT-MD simulations (2.66–2.80 D). This feature may be prototypical of the system we are modeling (a single molecule in a MM environment), since a similar underestimation (2.39 D) has been found in a previous

QM/MM study using a different electrostatic coupling scheme.<sup>67</sup>

However, our results clearly indicate that the DFT molecule is effectively polarized by its environment and should therefore behave like a liquid methanol molecule rather than like an isolated one. Again the influence of the functional is difficult to assess given the large standard deviations, but the CP2K protocol appears to provide dipole moments in better agreement with the experiment than CPMD, even if the difference is small. This behavior is due to the different nature of QM/MM coupling schemes and presumably to the different quality of  $r_c$  parameters that affects the average O...H distances, as discussed above.

Computation of the O–D stretching frequency also indicates that the DFT represented molecule is properly influenced by the environment since  $\tilde{\nu}_{\text{O-D}}$  ranges from 2501 to 2564  $\text{cm}^{-1}$ , in qualitative agreement with the experimental value for liquid methanol (2491  $\text{cm}^{-1}$ ; see Table 4 and Figure 3).<sup>31</sup> As in the gas phase, the best description is provided by BP86, BP86-D2, and BLYP (CPMD), but the two CP2K protocols lead to overestimated values (2564 and 2653  $\text{cm}^{-1}$  with BLYP and B97-D2, respectively) in solution. This result may be correlated with the exaggerated number of MM molecules surrounding each O<sub>DFT</sub> atom, as evidenced by the O–H<sub>o</sub> RDFs (see Table 2). We note that the nature of the QM/MM coupling should not be the only factor since some deviations from the experiment were already found in the gas phase with BLYP and B97-D2 (CP2K). All in all, our results show that the gas-to-liquid red shift can be qualitatively described by DFT/MM simulations, and that the DFT represented monomer thus effectively behaves like a liquid methanol molecule. A more accurate prediction of vibrational data should involve a more accurate model, and full DFT-MD would be preferred in this case.

## CONCLUSIONS

We have performed a benchmark study of four protocols to describe liquid methanol under ambient conditions by DFT-based molecular dynamics simulations. Full DFT and hybrid DFT/MM approaches have been considered within two popular implementations of *ab initio* molecular dynamics (CPMD and CP2K). Careful comparisons with the experiments have been made, considering four criteria to evaluate the extent to which the model solution effectively behaves like a liquid phase. Because the results of DFT-MD simulations can strongly depend on the choice of simulation parameters,<sup>24</sup> we took here special care to perform consistent comparisons between the different protocols, and identical parameters were employed within a given series of systems (i.e., the temperature, thermostats, time step, fictitious mass of the electrons, pseudopotentials, time step, etc.). Our results showed that full DFT-MD systematically yields an overstructured liquid that diffuses too slowly. The addition of a dispersion correction seems to be beneficial to improving the transport properties of the liquid in the case of BLYP, in keeping with recent results for liquid water.<sup>15</sup> Despite a too sluggish liquid being afforded, the model solutions do not seem to reach a “glassy” state within the time scale of our simulations (tens of picoseconds). To balance the sluggish behavior of methanol, increasing the temperature could be therefore recommended for practical use. Interestingly, induced polarization effects are well described with all functionals and protocols. Vibrational properties are qualita-

tively well described despite a tendency to underestimate the O–D stretching frequency by *ca.* 50  $\text{cm}^{-1}$ .

On the other hand, B97-D2 appears to perform particularly well, since this functional affords a softer structure and provides a better description of the O–D stretching mode in the liquid. Moreover, diffusion properties are also improved compared to the widely used BLYP functional, and induced polarization effects are also well described. These features are confirmed herein by considering a larger system of 64 molecules, and by extending a simulation up to 44 ps. The good performance of B97-D2 to describe liquid methanol may thus open the door to future modeling studies of solutions of transition metal complexes, where this functional also performs particularly well.<sup>20</sup> However, we should stress that such protocols (based on full DFT-MD) still remain computationally intensive, and practically, one would still be very limited by the size of simulated systems and by the length of the simulations.

In this context, hybrid DFT/MM molecular dynamics is found to be an attractive, computationally efficient, alternative, since a single DFT molecule is influenced reasonably well by the MM environment and effectively behaves like a liquid molecule (in terms of polarization and  $\tilde{\nu}_{\text{O-D}}$  stretching frequency). Induced polarization effects and average organization of the surrounding liquid is described with less accuracy than with full DFT-MD, but the method still captures most of the effect of the environment. We therefore conclude that our DFT/MM-MD protocols could be potentially employed to model chemical reactivity of systems in explicit solvent and should still outperform static methods based on polarizable continuum models. Improvements could be made by fine-tuning the empirical parameters involved in the QM/MM coupling, or, more promising, by increasing the size of the DFT region to include few neighboring methanol molecules. Given the fast hydrogen bonding dynamics in the liquid<sup>13d</sup> this should be done in a flexible way, i.e., following an adaptive QM/MM scheme as recently developed,<sup>68</sup> where molecules can smoothly cross the QM/MM boundary. Tests on the application of this approach are currently underway in our group.

## ASSOCIATED CONTENT

### Supporting Information

Methodological tests for the computation of WFCs with different functionals (Tables S1–S2). Details on the characteristics of the MD (Figure S1) and on the computation of the  $s_p$  scaling factor (Figure S2). VDOS in the 1600–3000  $\text{cm}^{-1}$  and 375–1350  $\text{cm}^{-1}$  domains are also provided (Figure S3 and S4, respectively). This material can be downloaded free of charge via the Internet at <http://pubs.acs.org>.

## AUTHOR INFORMATION

### Corresponding Author

\*E-mail: [nicolas.sieffert@ujf-grenoble.fr](mailto:nicolas.sieffert@ujf-grenoble.fr).

### Notes

The authors declare no competing financial interest.

## ACKNOWLEDGMENTS

This work was carried out under the HPC-EUROPA2 project (project number: 228398) with the support of the European Commission Capacities Area—Research Infrastructures Initiative. This work made use of the facilities of HECToR, the U.K.’s national high-performance computing service, which is provided by UoE HPCx Ltd. at the University of Edinburgh,



Cray Inc., and NAG Ltd. and funded by the Office of Science and Technology through EPSRC's High End Computing Programme. This work was granted access to the HPC resources of IDRIS under the allocations 2011-i2011086670 and 2012-i2011086670 made by GENCI (Grand Equipement National de Calcul Intensif). The authors also wish to thank EaStCHEM for support and access to the EaStCHEM Research Computing Facility and Dr. H. Früchtel for technical support. N.S. also thanks the UJF and the CNRS for funding, Prof. Leonardo Guidoni for his help with the CPMD/GROMOS96 interface, and Dr. Christian Philouze for interesting discussions.

## REFERENCES

- (1) Ahmed, M.; Dincer, I. *Int. J. Energy Res.* **2011**, *35*, 1213.
- (2) Ludwig, R. *ChemPhysChem* **2005**, *6*, 1369.
- (3) Blandamer, M. J.; Burgess, J. *Transition Met. Chem.* **1988**, *13*, 1.
- (4) Chaumont, A.; Wipff, G. *Phys. Chem. Chem. Phys.* **2008**, *10*, 6940.
- (5) Bühl, M.; Sieffert, N.; Chaumont, A.; Wipff, G. *Inorg. Chem.* **2011**, *50*, 299.
- (6) (a) Jorgensen, W. L. *J. Am. Chem. Soc.* **1980**, *102*, 543. (b) Jorgensen, W. L. *J. Phys. Chem.* **1986**, *90*, 1276.
- (7) Haughey, M.; Ferrario, M.; McDonald, I. R. *J. Phys. Chem.* **1987**, *91*, 4934.
- (8) (a) Dang, L. X.; Chang, T.-M. *J. Chem. Phys.* **2003**, *119*, 9851. (b) Patel, S.; Brooks, Iii, C. L. *J. Chem. Phys.* **2005**, *122*, 024508. (c) Ishiyama, T.; Sokolov, V. V.; Morita, A. *J. Chem. Phys.* **2011**, *134*, 024509.
- (9) Nielson, K. D.; van Duin, A. C. T.; Oxgaard, J.; Deng, W.-Q.; Goddard, W. A. *J. Phys. Chem. A* **2004**, *109*, 493.
- (10) See for instance the case of hydrogen transfer at a ruthenium center: Handgraaf, J.-W.; Meijer, E. J. *J. Am. Chem. Soc.* **2007**, *129*, 3099.
- (11) (a) Bühl, M.; Kabrede, H. *J. Chem. Theory Comput.* **2006**, *2*, 1282. (b) Waller, M. P.; Braun, H.; Hojdis, N.; Bühl, M. *J. Chem. Theory Comput.* **2007**, *3*, 2234. (c) Bühl, M.; Reimann, C.; Pantazis, D. A.; Bredow, T.; Neese, F. *J. Chem. Theory Comput.* **2008**, *4*, 1449.
- (12) Zhao, Y.; Truhlar, D. G. *J. Chem. Theory Comput.* **2011**, *7*, 669.
- (13) (a) Handgraaf, J.-W.; van Erp, T. S.; Meijer, E. J. *J. Chem. Phys. Lett.* **2003**, *367*, 617. (b) Handgraaf, J.-W.; Meijer, E. J.; Gaigeot, M.-P. *J. Chem. Phys.* **2004**, *121*, 10111. (c) Kuo, I. F. W.; Mundy, C. J.; McGrath, M. J.; Siepmann, J. I. *J. Phys. Chem. C* **2008**, *112*, 15412. (d) Pagliai, M.; Cardini, G.; Righini, R.; Schettino, V. *J. Chem. Phys.* **2003**, *119*, 6655. (e) Morrone, J. A.; Tuckerman, M. E. *J. Chem. Phys.* **2002**, *117*, 4403.
- (14) (a) Grimme, S. *J. Comput. Chem.* **2004**, *25*, 1463. (b) Grimme, S. *J. Comput. Chem.* **2006**, *27*, 1787. (c) Grimme, S.; Antony, J.; Ehrlich, S.; Krieg, H. *J. Chem. Phys.* **2010**, *132*, 154104.
- (15) (a) Lin, I. C.; Seitsonen, A. P.; Coutinho-Neto, M. c. D.; Tavernelli, I.; Rothlisberger, U. *J. Phys. Chem. B* **2009**, *113*, 1127. (b) Lin, I. C.; Seitsonen, A. P.; Tavernelli, I.; Rothlisberger, U. *J. Chem. Theory Comput.* **2012**, *8*, 3902–3910. (c) Jonchiere, R.; Seitsonen, A. P.; Ferlat, G.; Saitta, A. M.; Vuilleumier, R. *J. Chem. Phys.* **2011**, *135*, 154503.
- (16) Yoo, S.; Xantheas, S. S. *J. Chem. Phys.* **2011**, *134*, 121105.
- (17) Improvements to the average structure of supercritical CO<sub>2</sub> has also been reported using a different approach for the description of dispersion effects. See: Balasubramanian, S.; Kohlmeier, A.; Klein, M. L. *J. Chem. Phys.* **2009**, *131*, 144506.
- (18) McGrath, M. J.; Kuo, I. F. W.; Ghogomu, J. N.; Mundy, C. J.; Siepmann, J. I. *J. Phys. Chem. B* **2011**, *115*, 11688.
- (19) McGrath, M. J.; Kuo, I. F. W.; Siepmann, J. I. *Phys. Chem. Chem. Phys.* **2011**, *13*, 19943.
- (20) (a) Sieffert, N.; Bühl, M. *Inorg. Chem.* **2009**, *48*, 4622. (b) Minenkov, Y.; Singstad, A.; Occhipinti, G.; Jensen, V. R. *Dalton Trans.* **2012**, *41*, 5526.
- (21) Senn, H. M.; Thiel, W. *Ang. Chem. Int. Ed.* **2009**, *48*, 1198.
- (22) VandeVondele, J.; Mohamed, F.; Krack, M.; Hutter, J.; Sprik, M.; Parrinello, M. *J. Chem. Phys.* **2005**, *122*, 014515.
- (23) Kuo, I. F. W.; Mundy, C. J.; McGrath, M. J.; Siepmann, J. I. *J. Chem. Theory Comput.* **2006**, *2*, 1274.
- (24) Kuo, I. F. W.; Mundy, C. J.; McGrath, M. J.; Siepmann, J. I.; VandeVondele, J.; Sprik, M.; Hutter, J.; Chen, B.; Klein, M. L.; Mohamed, F.; Krack, M.; Parrinello, M. *J. Phys. Chem. B* **2004**, *108*, 12990.
- (25) (a) Laio, A.; VandeVondele, J.; Rothlisberger, U. *J. Chem. Phys.* **2002**, *116*, 6941. (b) Laio, A.; VandeVondele, J.; Rothlisberger, U. *J. Phys. Chem. B* **2002**, *106*, 7300.
- (26) (a) Laino, T.; Mohamed, F.; Laio, A.; Parrinello, M. *J. Chem. Theory Comput.* **2005**, *1*, 1176. (b) Laino, T.; Mohamed, F.; Laio, A.; Parrinello, M. *J. Chem. Theory Comput.* **2006**, *2*, 1370.
- (27) (a) Yamaguchi, T.; Hidaka, K.; Soper, A. K. *Mol. Phys.* **1999**, *96*, 1159. (b) *Mol. Phys.* **1999**, *97*, 603 Erratum.
- (28) Holz, M.; Mao, X.-a.; Seiferling, D.; Sacco, A. *J. Chem. Phys.* **1996**, *104*, 669.
- (29) McClellan, A. L., *Tables of Experimental Dipole Moment*; Rahara Enterprises, El Cerrito, CA (1989), as cited in: Dang, L. X.; Chang, T.-M. *J. Chem. Phys.* **2003**, *119*, 9851.
- (30) Serrallach, A.; Meyer, R.; Günthard, H. H. *J. Mol. Spectrosc.* **1974**, *52*, 94.
- (31) Bertie, J. E.; Zhang, S. L. *J. Mol. Struct.* **1997**, *413–414*, 333.
- (32) (a) Pearlman, D. A.; Case, D. A.; Caldwell, J. W.; Ross, W. S.; Cheatham Iii, T. E.; DeBolt, S.; Ferguson, D.; Seibel, G.; Kollman, P. *Comput. Phys. Commun.* **1995**, *91*, 1. (b) Case, D. A.; Cheatham, T. E.; Darden, T.; Gohlke, H.; Luo, R.; Merz, K. M.; Onufriev, A.; Simmerling, C.; Wang, B.; Woods, R. J. *J. Comput. Chem.* **2005**, *26*, 1668.
- (33) (a) Darden, T.; York, D.; Pedersen, L. *J. Chem. Phys.* **1993**, *98*, 10089. (b) Essmann, U.; Perera, L.; Berkowitz, M. L.; Darden, T.; Lee, H.; Pedersen, L. G. *J. Chem. Phys.* **1995**, *103*, 8577. (c) Ewald, P. P. *Annalen der Physik* **1921**, *369*, 253. (d) Laino, T.; Hutter, J. *J. Chem. Phys.* **2008**, *129*, 074102. (e) Toukmaji, A. Y.; Board, J. A. *Comput. Phys. Commun.* **1996**, *95*, 73.
- (34) The experimental density of liquid methanol at P = 1.01325 bar is 24.79141 mol/L at T = 290 K, and 24.49774 mol/L at T = 300 K (see: Goodwin, R. D. *J. Phys. Chem. Ref. Data* **1987**, *16*, 799). In our study, the densities considered in the simulated systems are 24.75 mol/L (32 methanol molecules, cell length 12.9 Å), 24.53 mol/L (64 molecules, 16.3 Å) and 23.47 mol/L (1367 molecules, 45.9 Å).
- (35) Case, D.A.; Darden, T.A.; Cheatham, T.E.; , III, Simmerling, C.L.; Wang, J.; Duke, R.E.; Luo, R.; Crowley, M.; Walker, R.C.; Zhang, W.; Merz, K.M.; Wang, B.; Hayik, S.; Roitberg, A.; Seabra, G.; I. Kolossvay, Wong, K.F.; Paesani, F.; Vanicek, J.; Wu, X.; Brozell, S.R.; Steinbrecher, T.; Gohlke, H.; Yang, L.; Tan, C.; Mongan, J.; Hornak, V.; Cui, G.; Matthews, D.H.; Seetin, M.G.; Sagui, C.; Babin, V.; , Kollman, P.A. (2008), AMBER 10, University of California, San Francisco.
- (36) (a) Nosé, S. *J. Chem. Phys.* **1984**, *81*, 511. (b) Martyna, G. J.; Klein, M. L.; Tuckerman, M. *J. Chem. Phys.* **1992**, *97*, 2635. (c) Hoover, W. G. *Phys. Rev. A* **1985**, *31*, 1695.
- (37) Note that only positions have been used from classical pre-equilibration. DFT and DFT/MM simulations are started from random velocities
- (38) (a) Car, R.; Parrinello, M. *Phys. Rev. Lett.* **1985**, *55*, 2471. (b) CPMD Version 3.15.1, Copyright IBM Corp. 1990–2006, Copyright MPI für Festkörperforschung Stuttgart, 1997–2001
- (39) (a) Becke, A. D. *Phys. Rev. A* **1988**, *38*, 3098. (b) Lee, C.; Yang, W.; Parr, R. G. *Phys. Rev. B* **1988**, *37*, 785.
- (40) (a) Perdew, J. P. *Phys. Rev. B* **1986**, *33*, 8822. (b) Perdew, J. P. *Phys. Rev. B* **1986**, *34*, 7406.
- (41) Troullier, N.; Martins, J. L. *Phys. Rev. B* **1991**, *43*, 1993.
- (42) Kleinman, L.; Bylander, D. M. *Phys. Rev. Lett.* **1982**, *48*, 1425.
- (43) VandeVondele, J.; Krack, M.; Mohamed, F.; Parrinello, M.; Chassaing, T.; Hutter, J. *Comput. Phys. Commun.* **2005**, *167*, 103.
- (44) For more information on CP2K see: <http://www.cp2k.org> (accessed October 17, 2012)
- (45) Schafer, A.; Huber, C.; Ahlrichs, R. *J. Chem. Phys.* **1994**, *100*, 5829.

- (46) (a) Goedecker, S.; Teter, M.; Hutter, J. *Phys. Rev. B* **1996**, *54*, 1703. (b) Hartwigsen, C.; Goedecker, S.; Hutter, J. *Phys. Rev. B* **1998**, *58*, 3641. (c) Krack, M. *Theor. Chem. Acc.* **2005**, *114*, 145.
- (47) Note that the importance of using diffuse basis sets and large cutoffs has already been discussed elsewhere in the literature (see e.g. the case of neat water in: ref 15c (and references cited therein). In the case of methanol, see e.g. references 18 and 19.
- (48) (a) Becke, A. D. *Phys. Rev. A* **1988**, *38*, 3098. (b) Perdew, J. P. *Phys. Rev. B* **1986**, *33*, 8822. (c) Perdew, J. P. *Phys. Rev. B* **1986**, *34*, 7406.
- (49) This convergence criterion is sufficient to achieve a good conservation of the energy. This is shown by pursuing the MD simulation of 32 methanol molecules (B97-D2) for 11 ps in the NVE ensemble, after 14 ps of pre-equilibration in the NVT ensemble. Time evolutions of the temperature and of the total energy (NVE) are given in Figure S1, and shows that the drift is effectively very small (ca.  $2.44 \times 10^{-6}$  H over 11 ps, i.e. ca.  $10^{-9}$  a.u./atom/ps).
- (50) Scott, W. R. P.; Hünenberger, P. H.; Tironi, I. G.; Mark, A. E.; Billeter, S. R.; Fennen, J.; Torda, A. E.; Huber, T.; Krüger, P.; van Gunsteren, W. F. *J. Phys. Chem. A* **1999**, *103*, 3596.
- (51) In practice, we employ the NVE ensemble for the study of vibrational properties of solutes (see Ref 59), whereas we employ the NVT ensemble for full DFT-MD studies of metal complexes in solution (see e.g. Bühl, M.; Sieffert, N.; Wipff, G. *Chem. Phys. Lett.* **2009**, *467*, 287). We therefore decided herein to test and validate our protocols in the same conditions, in view with their further applications.
- (52) More details can be found in the original papers of the CPMD and CP2K QM/MM implementations, see references 25 and 26, respectively.
- (53) Martyna, G. J.; Tuckerman, M. E. *J. Chem. Phys.* **1999**, *110*, 2810.
- (54) Humphrey, W.; Dalke, A.; Schulten, K. *J. Molec. Graphics* **1996**, *14*, 33.
- (55) Allen, M. P.; Tildesley, D. J. *Computer Simulation of Liquids*; Clarendon Press: Oxford, 1987.
- (56) Marzari, N.; Vanderbilt, D. *Phys. Rev. B* **1997**, *56*, 12847.
- (57) Silvestrelli, P. L.; Parrinello, M. *J. Chem. Phys.* **1999**, *111*, 3572.
- (58) Gaigeot, M.-P.; Sprik, M. *J. Phys. Chem. B* **2003**, *107*, 10344.
- (59) A detailed description of the method we employed to compute IR spectra from DFT-MD simulations can be found in: Gaigeot, M.-P. *Phys. Chem. Chem. Phys.* **2010**, *12*, 3336.
- (60) see e.g. Ong, S. W.; Tok, E. S.; Kang, H. C. *Phys. Chem. Chem. Phys.* **2010**, *12*, 14960.
- (61) We note that Cardini et al. followed a similar approach, as they employed a scaling factor of 1.0975 in conjunction with a fictitious mass of the electrons of 800 u.a. See: ref 13d.
- (62) Ivash, E. V.; Dennison, D. M. *J. Chem. Phys.* **1953**, *21*, 1804.
- (63) The differences observed when going from one functional to another also show on harmonic vibrational frequencies as obtained from static calculations in the gas phase. For example, we found  $2697 \text{ cm}^{-1}$  with BLYP and  $2750 \text{ cm}^{-1}$  with B97-D2. These values have been obtained by optimizing a (fully deuterated) methanol molecule in the gas phase using the def2-QZVPP basis set and computing the numerical frequencies with the Turbomole package. See: TURBOMOLE V6.4 2012, a development of University of Karlsruhe and Forschungszentrum Karlsruhe GmbH, 1989–2007, TURBOMOLE GmbH, since 2007; available from <http://www.turbomole.com> (accessed October 17, 2012).
- (64) Note that some other peaks are affected in the lower frequency spectrum such as the C-O stretching (labelled  $\nu_7$ ; see Figure S4). Such an underestimation has already been reported by Pagliai et al. with BLYP/CPMD (See ref 13d). We found that this shift is less important with B97-D2, BP86 and BP86-D2 compared to BLYP and its dispersion-corrected variants.
- (65) (a) Grabowski, S. C. *J. Chem. Rev.* **2011**, *111*, 2597. (b) Kollman, P. A.; Allen, L. C. *Chem. Rev.* **1972**, *72*, 283.
- (66) Morrone, J. A.; Tuckerman, M. E. *Chem. Phys. Lett.* **2003**, *370*, 406.
- (67) Tu, Y.; Laaksonen, A. *Phys. Rev. E* **2001**, *64*, 026703.
- (68) (a) Rode, B.; Hofer, T.; Randolph, B.; Schwenk, C.; Xenides, D.; Vchirawongkwin, V. *Theor. Chem. Acc.* **2006**, *115*, 77. (b) Bulo, R. E.; Ensing, B.; Sikkema, J.; Visscher, L. *J. Chem. Theory Comput.* **2009**, *5*, 2212. (c) Pezeshki, S.; Lin, H. *J. Chem. Theory Comput.* **2011**, *7*, 3625. (d) Bernstein, N.; Varnai, C.; Solt, I.; Winfield, S. A.; Payne, M. C.; Simon, I.; Fuxreiter, M.; Csanyi, G. *Phys. Chem. Chem. Phys.* **2012**, *14*, 646.